AJNR

MR Angiography of Dural Arteriovenous Fistulas: Diagnosis and Follow-Up after Treatment Using a Time-Resolved 3D Contrast-Enhanced Technique

S. Meckel, M. Maier, D. San Millan Ruiz, H. Yilmaz, K. Scheffler, E.-W. Radue and S.G. Wetzel

AJNR Am J Neuroradiol 2007, 28 (5) 877-884
http://www.ajnr.org/content/28/5/877

ORIGINAL RESEARCH

MR Angiography of Dural Arteriovenous Fistulas: Diagnosis and Follow-Up after Treatment Using a Time-Resolved 3D Contrast-Enhanced Technique

S. Meckel
M. Maier
D. San Millan Ruiz
H. Yilmaz
K. Scheffler
E.-W. Radue
S.G. Wetzel

BACKGROUND AND PURPOSE: Digital subtraction angiography (DSA) is the method of reference for imaging of dural arteriovenous fistula (DAVF). The goal of this study was to analyze the value of different MR images including 3D contrast-enhanced MR angiography (MRA) with a high temporal resolution in diagnostic and follow-up imaging of DAVFs.

MATERIALS AND METHODS: A total of 18 MR/MRA examinations from 14 patients with untreated ($n = 9$) and/or treated ($n = 9$) DAVFs were evaluated. Two observers assessed all MR and MRA investigations for signs indicating the presence of a DAVF, for fistula characteristics such as fistula grading, location of fistulous point, and fistula obliteration after treatment. All results were compared with DSA findings.

RESULTS: On time-resolved 3D contrast-enhanced (TR 3D) MRA, the side and presence of all patent fistulas ($n = 13$) were correctly indicated, and no false-positive findings were observed in occluded DAVFs ($n = 5$). Grading of fistulas with this imaging technique was correct in 77% and 85% of patent fistulas for both readers, respectively. On T2-weighted images, signs indicative of a DAVF were encountered only in fistulas with cortical venous reflux (56%), whereas on 3D time-of-flight (TOF) MRA, most fistulas (88%) were correctly detected. In complete fistula occlusion, false-positive findings were encountered on both T2-weighted images and on TOF MRA images.

CONCLUSION: In this study, TR 3D MRA proved reliable in detecting DAVFs and suitable for follow-up imaging. The technique allowed—within limitations—to grade DAVFs. Although 3D TOF MRA can depict signs of DAVFs, its value for follow-up imaging is limited.

Digital subtraction angiography (DSA) is the standard of reference for the diagnosis of dural arteriovenous fistula (DAVF) and for tailoring the appropriate treatment either by endovascular and/or surgical means. Apart from offering a high sensitivity and specificity in the detection of a DAVF, it enables the visualization of feeding arteries and the characterization of the venous drainage pattern. The latter determines the grading of DAVF, which is important for estimating the risk of clinical complications as well as for adopting the therapeutic strategy.[1-7] In treated patients, DSA allows the detection of residual arteriovenous shunts. However, this method remains an invasive tool, with a potential risk, albeit very low, of severe periprocedural complications,[8] as well as exposing both patients and medical staff to ionizing radiation.

Numerous MR imaging techniques have been applied for the detection of DAVF. On conventional MR, only a subset of DAVFs, that is high-grade fistulas, DAVFs with accompanying venoclusive disease, and DAVFs with complications, including infarction and hemorrhage, can be identified.[9-14] As reported recently 3D time-of-flight MRA (3D TOF MRA) has been shown to be more sensitive in diagnosing DAVF.[14-16] The major drawback of conventional MR investigations is the absence of any temporal resolution, which is necessary to appreciate the dynamic characteristics of a DAVF, such as anterograde or retrograde venous flow.

Received April 25, 2006; accepted after revision August 11.

From the Divisions of Neuroradiology (S.M., E.-W.R., S.G.W.) and Diagnostic Radiology (M.M.), Institute of Radiology, University Hospital, Basel, Switzerland; Neuroradiology Section (D.S.M.R., H.Y.), Department of Radiology and Medical Informatics, Geneva University Hospital, Geneva, Switzerland; MR Physics (K.S.), Institute of Radiology, University of Basel/University Hospital, Basel, Switzerland.

Address correspondence to Stephan Meckel, MD, Division of Neuroradiology, Institute of Radiology, University Hospital Basel, Petersgraben 4, 4031 Basel, Switzerland; e-mail: meckels@uhbs.ch.

Time-resolved contrast-enhanced MRA methods that allow a dynamic visualization of the contrast bolus passage through the cerebral vessels have shown to be promising techniques for assessing DAVFs, in that these introduce the dimension of temporal resolution to the imaging work-up. Heretofore, mainly 2D techniques have been applied in some series.[17-21] However, the projective nature of 2D images harbors several drawbacks, such as the necessity of repeated injections of contrast media in separately acquired planes, signal intensity cancellations along the slab, and superimposition of different vessels. The use of parallel imaging algorithms has enabled the development of 3D contrast-enhanced MRA techniques with high temporal resolution. The feasibility of this method for the assessment of cerebrovascular disease, foremost for the detection of arteriovenous malformation (AVM) and DAVF, has been demonstrated.[16,22-24] We hypothesized that this technique could be valuable for the pretherapeutic and posttherapeutic assessment of DAVFs.

Taking DSA images as the standard of reference, the goal of this study was to systematically analyze findings of DAVFs using 3 different MR images, namely time-resolved 3D contrast-enhanced MRA (TR 3D MRA), T2-weighted MR images, and 3D TOF MRA in a consecutive series of patients with DAVFs before and/or after treatment.

Materials and Methods

Patients

The imaging findings of 14 consecutive patients (6 women and 8 men), aged 38–78 years (mean age, 61.0 years) who underwent both MR and DSA in close succession for primary diagnosis of a DAVF or for follow-up evaluation of a treated DAVF were retrospectively analyzed. As part of our routine protocol, all MR examinations com-

prised a TR 3D MRA study, 3D TOF MRA, and standard spin-echo imaging sequences. A total of 18 MR/MRA and DSA examinations were divided into 2 groups: group 1 ($n = 9$), termed "initial diagnosis," consisted of examinations performed for diagnosis of a previously unknown DAVF. Group 2 ($n = 9$), termed "follow-up," included all follow-up evaluations after endovascular or surgical treatment of a DAVF. Endovascular treatment included transvenous embolization of dural sinuses with platinum coils and/or transarterial embolization by using polyvinyl alcohol (PVA) or silk fibers. Two examinations of the same patient, one before treatment and one during follow-up, were available for 4 patients. The time interval between MR/MRA imaging and DSA was variable (mean, 14.1 days; range, 0–196 days). It was 7 days or fewer in 14 cases, and >1 week in 4 cases. The latter 4 patients did not show clinical modification during the time interval between DSA and MR/MRA work-ups.

MR Protocol

MR imaging examinations were performed on a 1.5T scanner (Avanto; Siemens Medical Solutions, Erlangen, Germany) equipped with an SQ gradient system (slew rate, 200 T/s/m; gradient strength, 40 mT/m) using a 12-channel head coil.

TR 3D MRA. The TR 3D MRA technique used for this study was based on a 3D radio-frequency (rf)-spoiled fast low-angle shot (FLASH) sequence, as described previously.[22] A slab-selective rectangular rf pulse was applied for excitation, and gradient timing was optimized to yield the following scan parameters: TR, 1.74 ms; TE, 0.64 ms; flip angle α, 15°; bandwidth, 1220 Hz/pixel; FOV, 255 × 255 mm; matrix, 128 × 128; sections/slab, 56 (interpolated with section resolution = 64%); slab thickness, 123.2 mm; number of averages (NA), 1; phase resolution, 100%; phase partial Fourier factor, 6/8; and section partial Fourier factor, 6/8.

Parallel imaging was executed using the generalized autocalibrating partially parallel acquisition (GRAPPA) algorithm.[25] Besides spatial resolution (voxel volume) and signal acquisition time, signal-to-noise ratio in parallel imaging also depends on the spatial arrangement of the coil array (geometry factor g), the acceleration factor R, and the reconstruction algorithm.[26] Accordingly, increasing the acceleration factor results in a decrease in SNR, which parallels the increase in temporal resolution. With the given geometry of our 12-channel head coil, the SNR and reconstruction artifacts became critical beyond an acceleration factor of 6. An acceleration factor of 6 (acceleration factor of 3 and 30 reference lines along the phase encoding direction; acceleration factor of 2 and 16 reference lines along the partition encoding direction) was therefore selected as a trade-off between image quality and temporal resolution.[22]

The acquisition mode was sagittal with 29% section oversampling. Covering all arteries and veins of both hemispheres with these acquisitions, an in-plane resolution of 2.0 × 2.0 mm with a section thickness of 2.2 mm (after interpolation in section direction) and a temporal resolution of 1.5 seconds per 3D dataset were obtained. A single bolus of contrast agent (Gadovist 1.0; Schering, Baar, Switzerland) was administered using a power injector (10 mL, 3 mL/s). In total, a series of 25 3D datasets was acquired, where the acquisition of the first dataset was started simultaneously with the injection of the contrast agent bolus (TA = 37.5 seconds). The first acquisition was discarded, and the second dataset was used as a mask. Subsequent 3D volumes were subtracted by magnitude from this mask to remove any background signal intensity. Automated maximum intensity projection (MIP) reconstructions were generated in standard planes (coronal, sagittal). Reconstruction artifacts, such as residual folding or ringing, were not visible with an acceleration factor of 6 and using a 12-channel head coil.

T2-Weighted MR. Axial T2-weighted turbo spin-echo images were acquired in all patients as part of a standard MR imaging examination of the brain.

3D TOF MRA. 3D TOF MRA was performed with the following parameters: TR, 39 ms; TE, 5.21 ms; ramped flip angle α, 10–30°; nominal flip angle α, 20°; number of slabs, 3 (with 33.33% overlapping slabs); sections/slab, 30; section thickness, 1 mm; FOV, 200 × 167 mm; voxel size, 0.6 × 0.5 × 1 mm; number of averages, 1; venous presaturation pulse (thickness, 40 mm; gap, 10 mm), GRAPPA algorithm (acceleration factor of 2), and scan time of 4 minutes 38 seconds. The standard coverage of the slabs included the region from the foramen magnum to level of the roof of the ventricles.

Intra-arterial DSA

Diagnostic biplanar intra-arterial DSA (Axiom Artis BA; Siemens Medical Solutions) was performed after catheterization of the common, external, and internal carotid arteries and of the dominant vertebral arteries.

Evaluation

MR and MRA images of all patients were assessed on a 3D postprocessing workstation (Syngo; Siemens Medical Solutions). Images were independently analyzed by 2 experienced neuroradiologists (M.M and D.S.M.R) who were aware that all examinations were performed in patients with DAVFs. However, they were blinded to patients' history, clinical findings, results of DSA examinations, and the current state of the fistula (patent versus occluded). Both observers viewed sets of images, including all examinations of both groups of patients in a random fashion to reduce recall bias. Each set consisted of the images obtained with a given sequence displayed on a 3D workstation. There were 3 sets per patient (TR 3D MRA, axial T2-weighted MR, and 3D TOF MRA) that were evaluated at 3 different time points over a period of 2 months. 3D TOF MRA source images were displayed in multiplanar reformations allowing free-form interrogation and whole-brain or targeted MIP reconstructions along any desired obliquity. For the assessment of TR 3D MRA images, subtracted coronal and sagittal MIP reconstructions were used in a first step. In a second step, the observers had the opportunity of freewheeling assessment of subtracted 3D volumes as described for 3D TOF MRA. Both observers were forced to analyze the 3 different imaging modalities in a standardized fashion for the presence of "key" findings of a DAVF.

On TR 3D MRA images, the presence, the side (left, right, or midline), the venous segment of the fistulous point, the grading of the fistula, and the arterial feeders had to be determined. Early filling of a cerebral vein or a dural venous sinus was considered the diagnostic "key" finding of a DAVF. Venous segments were defined as follows: the superior sagittal sinus (SSS), the inferior sagittal sinus, the torcular of Herophili (ToH), the straight sinus, the vein of Galen, the transverse sinuses (TS), the sigmoid sinuses (SS), the jugular bulbs, the cavernous sinuses (CS), and cortical veins with detailed description. The type of shunt (direct cortical drainage versus shunt into a dural venous sinus), and signs of venous hypertension (retrograde flow inside a venous sinus or into a cortical vein, and cortical venous ectasia) were noted, and the DAVF was classified according to the system revised by Cognard et al.[1] The presence or absence of arterial feeders was evaluated using a semiquantitive score: 0, no visible feeding arteries; 1, suspected feeding artery (defined as an asymmetric appearance of an arterial branch that is located adjacent to the site of the

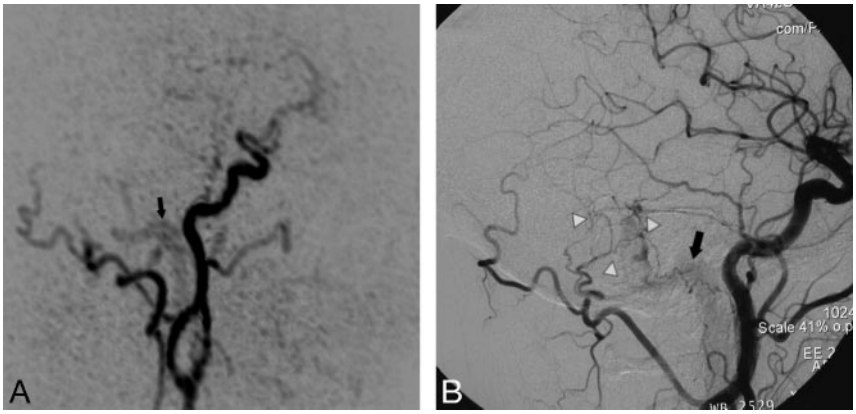

Fig 1. Targeted sagittal MIP reconstructed image of a TR MRA dataset obtained during early arterial phase (*A*) shows minimal venous filling of right sigmoid sinus (*black arrow*) in a patient with a low flow DAVF (type 1). The corresponding lateral DSA image with a right common carotid artery injection (*B*) demonstrates the fistula with mild early filling of right sigmoid sinus (*black arrow*) that is surrounded by a network of small feeding artery branches from the right occipital artery and middle meningeal artery (*white arrowheads*). This fistula was missed on 3D TOF MRA images.

fistula compared with the corresponding contralateral artery); and 2, confident findings of a feeding artery (defined as an arterial branch that shows a connection to an early filled venous structure). In addition, the number of feeding arteries detected with confidence (score 2) was noted.

On 3D TOF MRA images, as on TR 3D MRA images, the presence and the side of DAVF (left, right, or midline) and the venous segment of the fistulous point was noted. The delineation of vascular flow-related hyperintensities within a dural venous sinus or within a cortical vein, and/or the nodular or curvilinear hyperintensities located around a dural sinus, or near cerebral veins were regarded as the key findings to suspect a patent DAVF.[14-16] Whenever these signs were present, a determination was made whether focal congregations of transosseous vessels adjacent to the site of the fistula could be seen on source images. One examination of the group "initial diagnosis" was excluded because the fistulous point was located outside the scanned region. The grading of the DAVFs was not analyzed, because the 3D TOF MRA cannot provide information about contrast flow dynamics, which is the prerequisite for the classification system.[1] Moreover, because of limited spatial coverage and the lack of dynamic flow information an assessment of the feeding arteries was likewise not performed on 3D TOF MRA.

On T2-weighted images, only the presence and the side (left, right, or midline) of a DAVF was evaluated. A cluster of dural or leptomeningeal flow voids, venous ectasia or pouch, or regionally increased leptomeningeal flow voids were regarded as key findings of a suspected patent DAVF.[9-11,14] Other abnormalities, such as white matter hyperintensity and intracranial hemorrhage, were not considered possible indicators of the presence of a DAVF because these findings are unspecific and rather represent possible sequelae of fistulas.[10,11,13,14]

All DSA images were evaluated on hardcopies created from standard and superselective series of each examination. They were analyzed by 2 experienced interventional neuroradiologists (S.G.W., H.Y.) in consensus. Both were blinded to the results of MR and MRA investigations. The presence or absence of a DAVF, the exact location and side of the fistulous point, and the origin and the number of afferent feeding arteries were recorded (branches of the external and internal carotid arteries, or vertebral arteries). Venous drainage was analyzed with regard to the type of arteriovenous shunt (see above), and signs of venous hypertension (reflux into a dural sinus, or into a cortical vein, delayed general or regional venous filling, venous collaterals, and venous ectasia). All DAVFs were classified using the system proposed by Cognard et al.[1]

Data Analysis

The findings obtained by the 3 MR modalities were evaluated in comparison with the standard of reference, the DSA studies. For both groups, a descriptive analysis of the presence of a DAVF (TR 3D MRA and 3D TOF MRA), and arterial feeders (TR 3D MRA) was performed, and 95% binominal confidence intervals (95% CIs) were calculated for the frequencies of positive signs of a DAVF (SPSS; Chicago, Ill).

In addition, in a second analysis that included all patent DAVFs on conventional angiography, the grading on TR 3D MRA and the frequencies of positive findings suggestive of the presence of a fistula on 3D TOF MRA were evaluated. Weighted κ values were calculated for the agreement on grading (Cognard) between both observers, and separately between each observer, and the result from the corresponding DSA examination. κ values were also calculated for the agreement on different signs of a patent fistula on 3D TOF MRA.

Results

Description of DSA Findings

Group "Initial Diagnosis" ($n = 9$). DAVFs with antegrade venous flow (type 1) were found to be located at the TS/SS in 2 patients (Fig 1). DAVFs with moderate to severe venous hypertension (types 2a and 2a,b) at the level of the TS/SS were disclosed in 3 patients (Figs 2 and 3). Cortical fistulas with venous ectasia (type 4) were disclosed in 4 patients involving a temporal vein ($n = 1$), occipital cortical veins ($n = 2$), and a medial tentorial sinus ($n = 1$, Fig 4). In all fistulas, at least 2 separate feeding arteries were identified (range, 2–7).

Group "Follow-Up" ($n = 9$). Nine patients were evaluated during the follow-up after various endovascular or surgical treatments. These included 4 patients who were examined a second time after having undergone the above-reported diagnostic examination. One of these patients with a type 4 DAVF involving a medial tentorial sinus exhibited complete occlusion of fistula after surgery (Fig 4). In 2 patients, 1 harboring a type 2a fistula and the other a type 2a,b fistula involving the TS/SS, partial occlusion with down-staging of the fistulas to a benign grade (type 1) was achieved by endovascular transarterial and/or transvenous embolization procedures (Fig 2). In the fourth patient, a complex DAVF (type 2 a,b) at the ToH with multiple bilateral arterial feeders and severe cerebral venous outflow obstruction with occlusion of the straight sinus and left TS/SS, and postthrombotic narrowing of the

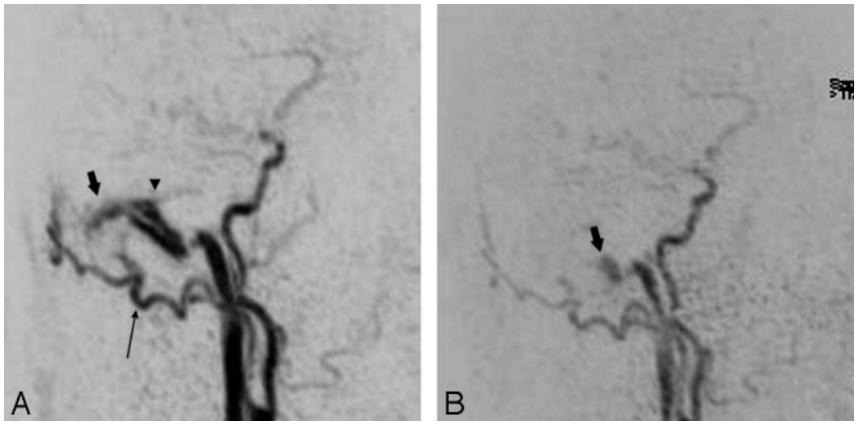

Fig 2. Preinterventional targeted MIP reconstructed sagittal image from an arterial phase of TR 3D MRA (*A*) shows a DAVF at the transverse/sigmoid sinus (*short arrow*) with strong early filling of the sinuses and feeding arterial branches from a prominent right occipital artery (*long arrow*). Small reflux into the proximal part of the vein of Labbé (*arrowhead*) is noted. The targeted MIP reconstructed image obtained from follow-up TR 3D MRA examination (*B*) after transvenous occlusion of the right transverse sinus clearly shows a residual fistula at the sigmoid sinus (*short arrow*) with downstaging of venous hypertension to anterograde sinus flow (type 1).

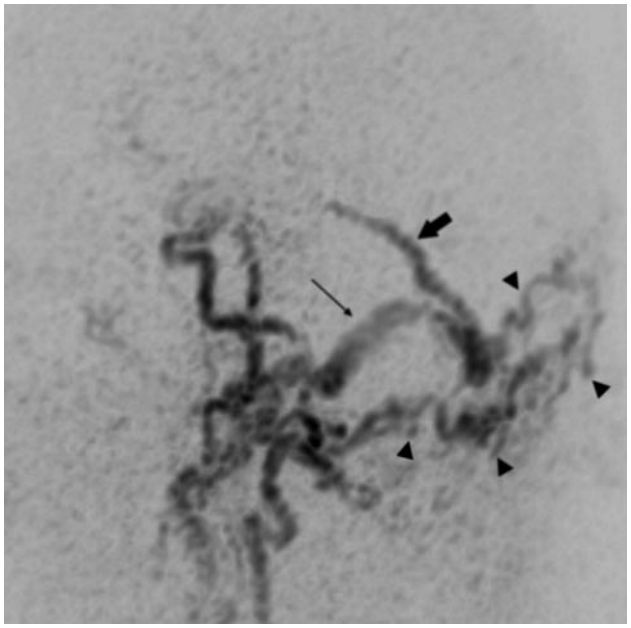

Fig 3. Sagittal targeted MIP reconstructed image obtained from an early arterial phase of TR 3D MRA shows a DAVF with strong and early filling of the torcular of Herophili, of the right transverse/sigmoid sinus (*long arrow*) and intense venous reflux into an enlarged superior vermian vein (*short arrow*) that follows the course of the tentorium in the midline. A large network of feeding branches from bilateral occipital arteries is observed (*arrowheads*).

SSS and the right TS was disclosed. Despite transarterial embolization procedures, a remarkable change in venous hemodynamics with persistent reflux into cortical veins did not occur (Fig 3).

In addition, 5 patients were exclusively examined during follow-up. Four of these patients had a complete occlusion of the fistulas. These included 3 DAVFs, located at the TS/SS/CS, that were treated with endovascular embolization procedures, and one patient with a type 4 fistula involving a cerebellar vein that had been excluded by surgery. In one patient with a DAVF involving the distal TS, a residual fistula with mild dural venous sinus reflux (type 2a) was observed despite transvenous and transarterial embolization.

Evaluation of Different MR/MRA Techniques

Group "Initial Diagnosis" ($n = 9$). Results of the assessment of the 3 MR modalities are summarized in Table 1.

TR 3D MRA. Both readers identified signs indicative of a DAVF in all 9 cases of angiographically proved fistulas. Both readers were able to identify correctly the location of the fistula for the given side in 9 DAVFs. Readers 1 and 2 detected correctly the given venous segment in 7 and 8 DAVFs, respectively. The wrongly specified venous segments comprised only DAVFs that involved a dural venous sinus. Results of the assessment of feeding arteries were as follows: No reader described false-positive feeding arteries in any fistula. No visible feeding artery (score 0) was encountered by any reader in 1 patient (11%). Reason to suspect an angiographically proved feeding artery (score 1) was found in 7 patients (78%) by reader 1 and in 4 patients by reader 2 (44%). Confident findings of an angiographically proved feeding artery (score 2) were observed in 2 patients by reader 1 (22%) and in 4 patients (44%) by reader 2. The occipital artery was most frequently disclosed as a feeder ($n = 7$). Two different feeding arteries were confidently identified in a single DAVF by reader 1 (11%) and in 2 DAVFs by reader 2 (22%). More than 2 separate feeding arteries were not identified.

3D TOF MRA. Signs indicative of a DAVF were found by both readers in 7 of 8 patients. Both readers missed one type 1 fistula at the sigmoid sinus (Fig 1). Readers 1 and 2 correctly estimated the side of the fistula on 3D TOF images in all 7 and in 6 of the 7 DAVFs, respectively. The venous segment of the suspected fistula was correctly identified in 3 of 7 and in 4 of 7 DAVFs by readers 1 and 2, respectively.

T2-Weighted MR. Signs indicative of a DAVF on axial T2-weighted images were detected by both readers in 5 of 9 DAVFs (Table 1) exclusively comprising fistulas with severe venous hypertension (types 2a,b and 4). Of these 5 patients, the location of the signs observed corresponded to the actual site of the fistulous point in only the 4 fistulas with direct cortical drainage (type 4). In 1 patient with a complex DAVF (type 2a,b), leptomeningeal flow voids were observed by both readers in widespread locations within the entire left cerebral hemisphere, the cerebellum, and the mesencephalic cisterns. The location of these findings did not match with the fistulous point (ToH) but with angiographically proved collateral venous channels.

Group "Follow-Up" ($n = 9$).

TR 3D MRA. In all patients ($n = 9$), both readers were able to differentiate between complete occlusion of a fistula and a patent residual fistula. The residual part of the fistula was correctly graded in 4 of 4 patients and in 3 of 4 patients by readers 1 and 2, respectively. This included 2 cases of down-staging to a type 1 fistula after endovascular therapy (Fig 2).

3D TOF MRA. The presence of a residual fistula was cor-

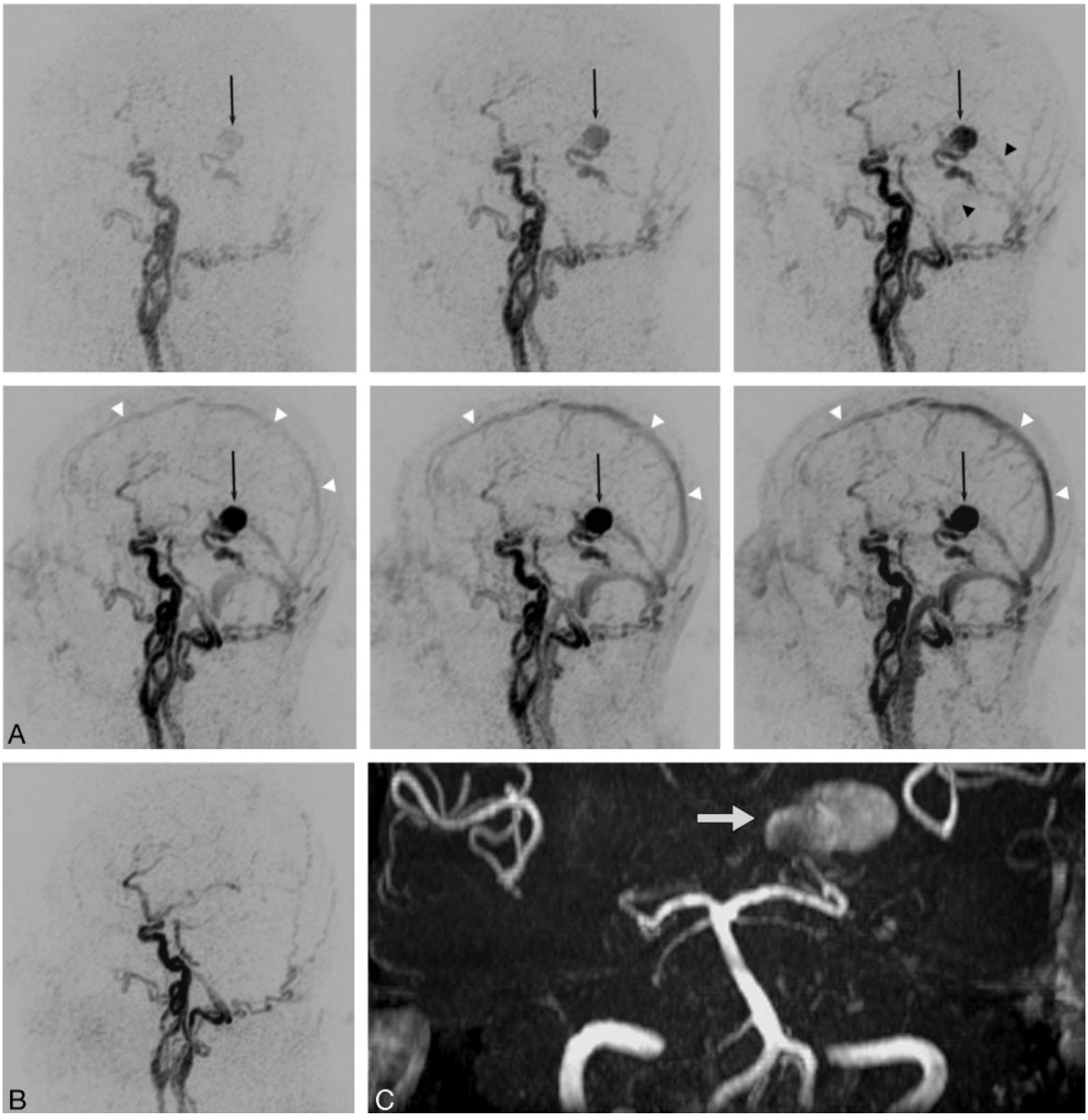

Fig 4. TR 3D MRA is obtained before and after surgical exclusion of a high-grade DAVF (type 4) on a left medial tentorial sinus. The complete arteriovenous series of sagittal MIP-reconstructed images (*A*) shows early enhancement of dilated veins with a large venous varix (*black arrow*) on the left tentorium at early arterial inflow (*top left*). Consecutive filling of the straight sinus and the transverse sinuses from the fistula is noted at later arterial phase (*top right, black arrowheads*). Regular temporal enhancement of the superior sagittal sinus (*white arrowheads*) can be appreciated during venous phases (*lower panel*). Note that fistula occlusion is definitely demonstrated by the absence of early filling of tentorial veins and varix on the follow-up study after surgery (*B*). On 3D TOF MRA, however, the venous varix (*white arrow*) is still depicted with a high signal intensity imitating fistula flow (*C*).

rectly indicated in 4 of 4 patients by both readers. However, residual fistulas were wrongly suspected in 2 surgically treated direct cortical fistulas of 3 (66%) that were proved to be completely occluded by DSA due to hyperintensities within a cortical vein and inside a large venous pouch (Fig 4).

T2-Weighted MR. Signs indicative of a DAVF were observed only in 1 of the 4 partially occluded DAVFs (type 2a,b fistula with accompanying postthrombotic obstruction of venous outflow). Of 5 completely occluded DAVFs, false-positive signs indicative of a residual fistula were disclosed in one case of an angiographically proved excluded type 4 DAVF on a medial tentorial sinus after surgery. In this case, tortuous dilated vessels on the tentorium with a hypointense signal intensity mimicking fistulous flow were encountered by both observers.

Analysis of Patent Fistulas

TR 3D MRA (n = 13). Grading of DAVFs was correct in 11 of 13 and in 10 of 13 fistulas by readers 1 and 2, respectively (Table 2). The agreement on fistula grading was very good between TR 3D MRA and DSA, with weighted κ values of 0.93 and 0.86 for observers 1 and 2, respectively. Interobserver agreement was also very good, with a weighted κ value of 0.86.

Table 1: Initial diagnosis of DAVFs on MR and MRA

	Presence of DAVF		Side of DAVF		Venous Segment of DAVF	
	Reader 1	Reader 2	Reader 1	Reader 2	Reader 1	Reader 2
T2-weighted MR (n = 9)	56% (21%–86%)	56% (21%–86%)	80% (28%–99%)	80% (28%–99%)	N/A	N/A
3D TOF MRA (n = 8*)	88% (47%–100%)	88% (47%–100%)	100% (65%–100%)	86% (42%–100%)	43% (10%–82%)	57% (18%–90%)
TR 3D MRA (n = 9)	100% (72%–100%)	100% (72%–100%)	100% (72%–100%)	100% (72%–100%)	78% (40%–97%)	89% (52%–100%)

Note:—DAVF indicates dural arteriovenous fistula; MRA, MR angiography. Data are presented as percentage of correct detection with 95% CIs in parentheses. If signs suggestive of a DAVF were not encountered on an examination it was subsequently excluded from the location analysis.
* One examination was excluded because the fistulous point was located outside the scanned region.

One observer wrongly upgraded 1 type 1 DAVF to type 2a, as did both observers in a second type 1 DAVF. One observer wrongly downgraded 1 type 2a DAVF to type 1, and 1 observer wrongly downgraded a type 2a,b DAVF to type 2a.

3D TOF MRA (n = 12). The frequencies of different signs suggestive for a DAVF were as follows: hyperintensities in sinuses or veins were encountered in 11 examinations (92%) by both readers (95% CI, 62%–100%) with an excellent interobserver agreement (κ value of 1.0; 95% CI, 100%), and hyperintense nodular or curvilinear structures around sinuses or veins in 7 examinations by reader 1 (58%; 95% CI, 28%–85%) and in 10 examinations by reader 2 (83%; 95% CI, 52%–98%) with a moderate interobserver agreement (κ value of 0.44; 95% CI, 0%–99%). Focally congregrated small transosseous vessels were observed in 9 examinations by reader 1 (75%; 95% CI, 43%–95%, and in 8 examinations by reader 2 (67%; 95% CI, 35%–90%), with a good interobserver agreement (κ value of 0.8; 95% CI, 43%–100%) (Fig 5).

Discussion

2D time-resolved contrast-enhanced MRA has proved to be valuable method to study the cerebral hemodynamics of DAVFs.[17-21] For the acquisition of different planes of projected images (axial, coronal, or sagittal), however, each projection can only be acquired with a separate injection of a contrast bolus increasing the total dose of contrast media. The best plane for visualization of an individual fistula may depend on the location of the fistula (eg, cavernous, sigmoid, tentorial).[21] Besides other limitations, such as signal intensity cancellations along a thick slab, mainly superimposition of different arterial and venous structures within a slab as a result of the projective nature of the images can impair the detection and exact characterization of a DAVF. By contrast, TR 3D MRA enables the generation of targeted or whole-brain 3D reconstructions in any desired obliquity of an acquired 3D volume.[22]

In our series of patients, TR 3D MRA provided a correct diagnosis of a patent DAVF in all cases and a correct differentiation between partially patent and occluded fistulas after treatment compared with DSA. In a previous report, 2 of 15 DAVFs were missed on TR 3D MRA datasets.[16] However, those negative findings might be partly related to the inferior spatial and temporal resolution used in that study, whereas partitions of 10-mm thickness with a temporal resolution of 4 s/dataset were used. Using parallel imaging, we were able to acquire nearly isovolumetric datasets at a high temporal resolution (1.5 seconds/dataset).

Nevertheless, it has to be acknowledged that both the temporal and spatial resolution of TR 3D MRA, as used in our implementation, were markedly inferior compared with DSA. Although all fistulas of our series were detected on TR 3D MRA, its voxel size of $2 \times 2 \times 2.2$ mm may potentially impair detection of small fistulas. Furthermore, apart from the detection of fistulas, this can hamper the visualization of small feeding arteries as a major shortcoming. Therefore, observers described only the the dominant feeding arteries, whereas on DSA, a minimum of 2 separate feeding arteries, and in most cases a network with different major and minor tributary arteries, was encountered. However, it is important to acknowledge that a detailed analysis of arterial feeders requires besides high spatial resolution selective, and at times superselective vessel injection on DSA. Moreover, the limited temporal and

Table 2: Grading of patent DAVFs (Cognard) on TR 3D MRA

	Correct Grading (%)	Weighted κ Values	95% Confidence Intervals (%)
Reader 1 vs. DSA	11/13 (85%)	0.93	52%–100%
Reader 2 vs. DSA	10/13 (77%)	0.86	40%–100%
Reader 1 vs. Reader 2	10/13 (77%)	0.86	40%–100%

Note:—DAVF indicates dural arteriovenous fistula; TR 3D MRA, time-resolved 3D MR angiography. Grading of DAVFs was performed according to the Cognard classification (6 types). All examinations that showed angiographically proved patent fistulas were included in this evaluation (n = 13). The interobserver agreement was determined by weighted κ values including 95% confidence intervals.

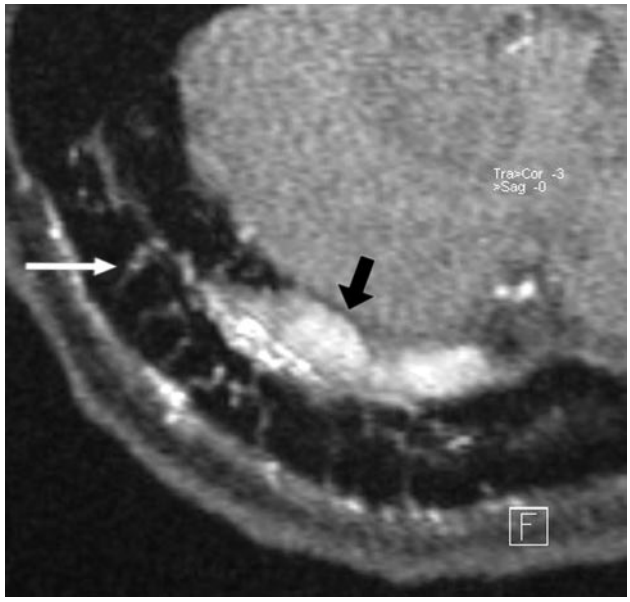

Fig 5. In a patient with a DAVF involving the right transverse sinus, transvenous coil occlusion of the distal part of the transverse sinus and the sigmoid sinus has been performed. A residual type 2a fistula at proximal part of the right transverse sinus with arterial feeders from the right occipital artery is demonstrated at follow-up imaging. The magnified axial source image of 3D TOF MRA shows multiple hyperintense thin transosseous vessels (*white arrow*) in the vicinity of the arterialized right transverse sinus (*black arrow*).

spatial resolution might mask reflux into small cortical veins and was most likely the reason for incorrect grading of fistulas compared with DSA. In fact, in high-flow DAVFs, particularly in those with venous reflux, a large segment of the venous sinus structures may enhance on the first "early arterial" image of the TR 3D MRA series. This effect can impair the determination of flow direction within a venous sinus and the exact localization of the fistulous point. However, despite these limitations, most fistulas were graded correctly. False specifications of grade differed in all cases by only one point on the Cognard scale, and distinct downgrading of fistulas during follow-up was correctly identified. Finally, although not analyzed in this study, discrimination of the exact type of fistulization (single hole versus network of small transdural shunts) may be impaired by the large voxel size.

3D TOF MRA was also a valuable tool for the initial diagnosis; only one low-flow fistula was missed. However, this technique has some important drawbacks: foremost, its value for follow-up imaging is questionable in that subacute intravascular thrombus can show high signal intensities within a cerebral vein that might mimic fistula flow in completely occluded DAVFs. "Static" TOF MRA was also inferior to TR 3D MRA with regard to precise location of fistula, because widespread hyperintensities that are particularly observed in DAVFs with venous reflux may be present in a large part of the sinuses and cortical veins adjacent to the fistulous point. Moreover, hyperintense signal intensity caused by passage of unsaturated flow may be a further limiting feature of the flow-sensitive TOF method, a finding that other investigators have observed in patients without DAVFs.[16] The limited spatial coverage of the standardized slabs did not allow the analysis of feeding arteries. In addition, no information about cerebral venous outflow can be obtained with this method. By contrast, TR 3D MRA provides venous phase images, which may disclose accompanying venous steno-occlusive disease as a result of thrombosis or postthrombotic changes. These findings were observed in some cases of DAVFs but were not a focus of this study. On the other hand, the voxel dimension of 3D TOF MRA is approximately 2–4 times greater than TR 3D MRA as implemented in our study. The higher spatial resolution can be exploited to depict small vessels that are involved in a fistula. Several signs have been described as being indicative of DAVFs on 3D TOF MRA images. Noguchi et al[16] reported that the finding of hyperintense nodular or curvilinear structures around a sinus showed the highest sensitivity and specificity in the diagnosis of a DAVF. We observed a higher frequency of findings of hyperintensity within venous sinuses or cerebral veins compared with the other signs that were analyzed in patent fistulas, which is in accordance with another recent report.[14] These divergent results may be attributed to different types of fistulas studied, because Noguchi et al did not examine either low-flow DAVFs or fistulas with direct cortical drainage. Furthermore, we encountered a high frequency of hyperintense transosseous vessels that are best visualized on TOF MRA source images—a finding that, until this point and to our best knowledge, had been described only in case observations.[27] Presumably representing small osteodural feeders originating from extracranial arteries, the frequency of this sign may be influenced by the type of arterial supply of a DAVF (meningeal arteries versus extracranial arteries). Finally, 3D TOF MRA that enables the visualization of small vessels involved in a fistula at comparatively higher spatial resolution and TR 3D MRA that provides important hemodynamic information about the AV-shunt may be used as complementary tools in a noninvasive work-up of DAVFs.

As we expected, clusters or regionally increased flow voids of dural or leptomeningeal vessels, as well as venous ectasia that are regarded as the key findings suggestive of a DAVF[9-11,14] appeared with a low frequency on T2-weighted MR images and did so exclusively in DAVFs with cortical venous drainage. It is also emphasized that the location of dilated veins does not necessarily correspond to the fistula network or the fistulous point, because extensive collateral flow networks remote from the site of the fistula can occur in postthrombotic conditions. This observation is consistent with a previous report.[12] Furthermore, after treatment hypointensities in veins might be wrongly interpreted as flow voids suggestive of residual fistula flow. In fact, an intravascular thrombosis after occlusion of a fistula might cause the signal intensity abnormality, which severely limits the value of this method for follow-up imaging. Standard T1-weighted images that are commonly acquired in routine examinations were not included in this study. On these images, subacute thrombus may be hyperintense similar to images of 3D TOF MRA. However, the signal intensity of thrombosis can be variable on standard spin-echo sequences with many overlaps between normal veins and thrombosis as a result of different breakdown stages of thrombosis, variable velocity of blood in normal cerebral veins, and flow-related enhancement.[28] Therefore, an unequivocal discrimination between residual fistula flow and complete occlusion may not be possible analyzing solely spin-echo images.

Our study has some important drawbacks. First, we did not conduct examinations of a control group of patients without DAVF to preclude observer bias. This bias, however, was reduced by the inclusion of occluded fistulas in the analysis. Second, treatment-related abnormalities caused by susceptibility artifacts from platinum coils or postoperative changes were evident in 6 of the patients on T2-weighted images and source images of 3D TOF MRA. However, the mere detection of treatment-related artifacts did not enable the reviewers to distinguish between fistula occlusion and residual arteriovenous shunts. In addition, such artifacts were not observed on TR 3D MRA as solely subtracted images were reviewed. Likewise, no relevant distortion of vascular appearance as a result of field warping associated with susceptibility artifacts was visible on those subtracted images. After transarterial embolization using silk fibers or PVA, such artifacts were not encountered on images of any MR/MRA sequence. Third, various cerebrovascular diseases that are associated with arteriovenous shunts, foremost pial AVMs, may produce similar findings on TR 3D MRA. Hence, the sensitivity and specificity of this technique remains to be established in further studies involving a larger number of subjects and including various cerebrovascular diseases. It would then be possible more clearly to define the role of TR 3D MRA in the investigative algorithm for patients with symptoms suggestive of a DAVF. Fourth, techniques of image acquisition that are known to improve the spatial and/or the temporal resolution, for instance combining parallel imaging and *k*-space sharing tech-

niques were not applied in this study.[24] Finally, applying high-field imaging (3T) could be advantageous by increasing the signal-to-noise ratio of TR 3D MRA images as demonstrated in a previous case observation of a DAVF.[23] However, such high-field MR scanners are not broadly available at the moment.

Conclusion

Early venous filling of a sinus or a cortical vein on images of TR 3D MRA were found to be reliable signs in detecting DAVFs, in both diagnostic and follow-up imaging. Moreover, TR 3D MRA proved superior to the other studied MR images for depicting fistula occlusion in DSA-proved complete obliteration and for downstaging in cases of DSA-proved residual fistulas after treatment. Other sequences such as T2-weighted images and 3D TOF MRA showed false-positive results relative to fistula occlusion. Whereas grading and localization of DAVFs on TR 3D MRA correlated well with DSA results, the detection of mild venous reflux and the delineation of small feeding arteries were less effective because of the relatively low spatial and temporal resolution compared with DSA. On 3D TOF MRA, the hyperintense visualization of cerebral venous structures was most frequently encountered in patent fistulas, followed by the hyperintense transosseous vessel sign.

The present results suggest that TR 3D MRA is an effective MR imaging tool in patients with the clinical suspicion of a DAVF and for follow-up after treatment of a DAVF. However, its exact role in the imaging algorithm for patients with suspicion of or proved DAVFs remains to be established. At least for the time being, DSA remains the method of preference for treatment planning and in cases of equivocal results on MRA.

References

1. Cognard C, Gobin YP, Pierot L, et al. **Cerebral dural arteriovenous fistulas: clinical and angiographic correlation with a revised classification of venous drainage.** *Radiology* 1995;194:671–80
2. Davies MA, TerBrugge K, Willinsky R, et al. **The validity of classification for the clinical presentation of intracranial dural arteriovenous fistulas.** *J Neurosurg* 1996;85:830–37
3. Borden JA, Wu JK, Shucart W. **A proposed classification for spinal and cranial dural arteriovenous fistulous malformations and implications for treatment.** *J Neurosurg* 1995;82:166–79
4. Klisch J, Huppertz HJ, Spetzger U, et al. **Transvenous treatment of carotid cavernous and dural arteriovenous fistulae: results for 31 patients and review of the literature.** *Neurosurgery* 2003;53:836–56
5. Goto K, Sidipratomo P, Ogata N, et al. **Combining endovascular and neurosurgical treatments of high-risk dural arteriovenous fistulas in the lateral sinus and the confluence of sinuses.** *J Neurosurg* 1999;90:289–99
6. Roy D, Raymond J. **The role of transvenous embolization in the treatment of intracranial dural arteriovenous fistulas.** *Neurosurgery* 1997;40:1133–44
7. Tomak PR, Cloft HJ, Kaga A, et al. **Evolution of the management of tentorial dural arteriovenous malformations.** *Neurosurgery* 2003;52:750–62
8. Cloft HJ, Joseph GJ, Dion JE. **Risk of cerebral angiography in patients with subarachnoid hemorrhage, cerebral aneurysm, and arteriovenous malformation: a meta-analysis.** *Stroke* 1999;30:317–20
9. De Marco JK, Dillon WP, Halbach VV, et al. **Dural arteriovenous fistulas: evaluation with MR imaging.** *Radiology* 1990;175:193–99
10. Willinsky R, Terbrugge K, Montanera W, et al. **Venous congestion: an MR finding in dural arteriovenous malformations with cortical drainage.** *AJNR Am J Neuroradiol* 1994;15:1501–07
11. Willinsky R, Goyal M, terBrugge K, et al. **Tortuous, engorged pial veins in intracranial dural arteriovenous fistulas: correlations with presentation, location, and MR findings in 122 patients.** *AJNR Am J Neuroradiol* 1999;20:1031–36
12. Hurst RW, Bagley LJ, Galetta S, et al. **Dementia resulting from dural arteriovenous fistulas: the pathologic findings of venous hypertensive encephalopathy.** *AJNR Am J Neuroradiol* 1998;19:1267–73
13. Seon-Kyu Lee, Willinsky RA, Montanera W, et al. **MR imaging of dural arteriovenous fistulas draining into cerebellar cortical veins.** *AJNR Am J Neuroradiol* 2003;24:1602–06
14. Kwon BJ, Han MH, Kang HS, et al. **MR imaging findings of intracranial dural arteriovenous fistulas: relations with venous drainage patterns.** *AJNR Am J Neuroradiol* 2005;26:2500–07
15. Chen JC, Tsuruda JS, Halbach VV. **Suspected dural arteriovenous fistula: results with screening MR angiography in seven patients.** *Radiology* 1992;183:265–71
16. Noguchi K, Melhem ER, Kanazawa T, et al. **Intracranial dural arteriovenous fistulas: evaluation with combined 3D time-of-flight MR angiography and MR digital subtraction angiography.** *AJR Am J Roentgenol* 2004;182:183–90
17. Wetzel SG, Bilecen D, Lyrer P, et al. **Cerebral dural arteriovenous fistulas: detection by dynamic MR projection angiography.** *AJR Am J Roentgenol* 2000;174:1293–95
18. Aoki S, Yoshikawa T, Hori M, et al. **MR digital substraction angiography for the assessment of cranial arteriovenous malformations and fistulas.** *AJR Am J Roentgenol* 2000;175:451–53
19. Klisch J, Strecker R, Hennig J, et al. **Time-resolved projection MRA: clinical application in intracranial vascular malformations.** *Neuroradiology* 2000;42:104–07
20. Coley SC, Romanowski CA, Hodgson TJ, et al. **Dural arteriovenous fistulae: non-invasive diagnosis with dynamic MR digital subtraction angiography.** *AJNR Am J Neuroradiol* 2002;23:404–07
21. Horie N, Morikawa M, Kitigawa N, et al. **2D thick-section MR digital subtraction angiography for the assessment of dural arteriovenous fistulas.** *AJNR Am J Neuroradiol* 2006;27:264–69
22. Meckel S, Mekle R, Taschner C, et al. **Time-resolved 3D contrast-enhanced MRA with GRAPPA on a 1.5 T system for imaging of cranio-cervical vascular disease: initial experience.** *Neuroradiology* 2006;48:291–99
23. Ziyeh S, Strecker R, Berlis A, et al. **Dynamic 3D MR angiography of intra- and extracranial vascular malformations at 3T: a technical note.** *AJNR Am J Neuroradiol* 2005;26:630–34
24. Tsuchiya K, Aoki C, Fujikaw A, et al. **Three-dimensional MR digital substraction angiography using parallel imaging and keyhole data sampling in cerebrovascular diseases: initial experience.** *Eur Radiol* 2004;14:1494–97
25. Griswold MA, Jakob PM, Heidemann RM, et al. **Generalized autocalibrating partially parallel acquisitions (GRAPPA).** *Magn Reson Med* 2002;47:1202–10
26. Pruessmann KP, Weiger M, Scheidegger MB, et al. **SENSE: sensitivity encoding for fast MRI.** *Magn Reson Med* 1999;42:952–62
27. Alatakis S, Koulouris G, Stuckey S. **CT demonstrated transcalvarial channels diagnostic of ural arteriovenous fistula.** *AJNR Am J Neuroradiol* 2005;26:2393–96
28. Liang L, Korogi Y, Sugahara T, et al. **Evaluation of the intracranial dural sinuses with a 3D contrast-enhanced MP-RAGE sequence: prospective comparison with 2D-TOF MR venography and digital subtraction angiography.** *AJNR Am J Neuroradiol* 2001;22:481–92